Proceedings of the 7th International Conference on Civil Structural and Transportation Engineering (ICCSTE'22)
Niagara Falls, Canada – June 05-07, 2022
Paper No. 160
DOI: 10.11159/iccste22.160

Nano-Modified Cementitious Composites Reinforced with Basalt Fiber Pellets for Repair/Overlay applications

Ahmed Azzam[1], Mohamed T. Bassuoni[2], Ahmed Shalaby[3]
[1]University of Manitoba and Ain Shams University
azzama@myumanitoba.ca
[2,3]University of Manitoba
[1,2,3]E1-368A EITC, 15 Gillson Street, Winnipeg, MB, Canada, R3T 5V6
mohamed.bassuoni@umanitoba.ca; ahmed.shalaby@umanitoba.ca

Abstract - There is a constant demand for high-performance materials to build and rehabilitate concrete infrastructure. The current study investigated the properties of nano-modified cementitious composites, incorporating emerging basalt fiber pellets (BFP), including their suitability as repair/overlay for concrete. The composites comprised 50% cement replacement with fly ash or slag, 6% nano-silica addition and two BFP dosages (2.5% and 4.5% by volume). The cementitious composites were assessed in terms of hardened properties, as well as their compatibility with parent concrete substrate. Furthermore, microstructural analyses were performed to evaluate the evolution of microstructure and interpret the bulk trends. The results showed that the composites had high strength, ductility, and resistance to infiltration of fluids. Moreover, BFP effectively contributed to the dimensional stability of the composites, which had high thermal and elastic compatibility with concrete substrate. Hence, the studied cementitious composites may offer an attractive alternative as high-performance repair/overlay materials for concrete infrastructures such as pavements and bridge decks.

***Keywords*:** Nano-silica; Basalt fiber pellets; Fly ash; Slag; Cementitous Composites; Repair; Overlay.

1. Introduction

Various rehabilitation and preventive maintenance techniques such as full or partial-depth repairs, joint sealing, and overlays, as well as types of materials (e.g., fiber-reinforced concrete, polymer-modified concrete, etc.) have been used to restore and/or improve the performance of concrete infrastructure [1,2]. Partial-depth repair replaces unsound concrete in the top one-third to one-half of concrete section (e.g., pavements, bridge decks), to restore its serviceability, and deter further deterioration [1,2]. Bonded overlays add structural capacity to concrete, conceal surface distresses of existing concrete that are in good to fair structural conditions, and mitigate damage caused by exposure to the environment and traffic loads (e.g. de-icing salts, and repeated loads) [2]. Accordingly, the repair/overlay is designed to deform monolithically with substrate concrete to ensure integrity of the composite section and load transfer between layers of the system [3,4].

Specifications of repair and overlay materials for concrete pavements and bridge decks [1,2] typically favour rapid strength gaining materials to minimize interruption to traffic. Many of these materials are vulnerable to cracking, poor bonding, and premature deterioration due to several factors including low ductility, and incompatibility with the existing concrete [e.g., 5]. Thus, the use of high-performance fiber-reinforced cementitious composites (HPFRCC) in repair/overlay applications can mitigate these technical challenges. Basalt fibers are a relatively new type of fibers, with high potential for the concrete industry due to its excellent mechanical properties (tensile strength of 3,000 - 4,000 MPa and modulus of elasticity of 93 - 110 GPa), non-corrosive nature, and low cost compared with other types of fibers (e.g., steel, glass) [6]. Nevertheless, they are vulnerable in alkaline media, which makes them susceptible to decomposition in cementitious matrices (pH of 11-13) within 90 days due to possible alkali-silica reactivity [7]. To mitigate such deficiency, one of the alternatives is to encapsulate basalt fiber strands in polymeric resins (e.g., vinyl-ester [8], polyamide [9]), hence developing a new class of fibers termed basalt fiber pellets (BFP). However, research on the use of BFP in concrete and cementitious composites is still at an early stage, which warrants further investigation to explore their suitability for multiple applications.

Extensive studies on supplementary cementitious materials (SCM), such as fly ash and slag, showed that their incorporation in cementitious binders generally enhances the hardened properties of concrete [e.g., 10]. The delay in setting time, strength gain, and microstructural development at early ages are considered the main deterrents for binders with high-volume SCM to be widely accepted as repair/overlay materials though [11]. Thereby, nanomaterials (e.g., nano-silica) have been used to alleviate the technical limitations of high-volume SCM [12]. Nano-modified HPFRCC comprising novel BFP have been developed at the University of Manitoba [10]. The binder comprised high content (50% by mass of binder) SCM with nano-silica addition (6%). The composites showed superior mechanical properties and adequate resistance to salt-frost scaling (according to ASTM C672/C672M [13]) [9, 14]. These findings are the primary motive for the present study. Hence, in this study, the authors investigated the suitability of nano-modified cementitious composites comprising BFP for repair/overlay of concrete infrastructures (e.g., pavements and bridge decks). The composites were integrally tested for mechanical properties, resistance to infiltration of fluids, as well as compatibility with substrate concrete. Such HPFRCC with balanced performance may present an attractive rehabilitation/protection option in heavy traffic zones.

2. Experimental Procedure

2.1. Materials and Mixtures

The base binders comprised 50% general use cement (GU) and 50% SCM, Type F fly ash or Grade 100 slag, in compliance with CAN/CSA-A3001 [15] to meet the requirement for high-volume supplementary cementitious materials (HVSCM-1) concrete, according to Annex K in CSA 23.1 [16]. A commercial nano-silica sol (NS) was added at a dosage of 6% by mass of the base binder. The colloid contains 50% well-dispersed NS particles in a water-based solution. The mean particle size of NS is 35 nm, and its pH, specific gravity, and specific surface are 9.5, 1.1 g/cm^3, and 80 m^2/g, respectively. Previous studies [e.g., 9] showed that 6% of this NS solution has a positive effect on the microstructural evolution and hardened properties of mortar/concrete with SCM. Continuously graded (0 to 600 μm) quartz sand with fineness modulus of 2.8 was used in the composites. The absorption and specific gravity of the sand are 1.5% and 2.6, respectively. High-range water-reducing admixture (HRWRA), poly-carboxylic acid-based, was used to achieve a target flow of 180±20 mm. The composites were reinforced with BFP (Fig. 1) at two different dosages of 2.5% and 4.5% by volume (equivalent to 1% and 2%, respectively basalt fibers by volume). The pellets are 36 mm in length and 1.8 mm in diameter with an aspect ratio of 20. They are made of 16-μm basalt roving encapsulated with polyamide resin (Nylon 6), and the fiber component represents 60% of the pellet by mass. BFP has a specific gravity of 1.74 with tensile strength and modulus of elasticity of 2300 MPa and 65 GPa, respectively. The formulations of the cementitious composites (Table 1) stem from high-performance concrete perspective that would be typically required for concrete repair/overlay systems [1,2]. The total content of the base/reference binders (GU cement and fly ash or slag) and nano-modified binders were 700 kg/m^3 and 742 kg/m^3, respectively, at a low *w/b* of 0.30.

Fig.1: Reinforcing basalt fiber pellets (BFP).

Table 1: Mixture proportions for the composites per cubic meter.

Mixture ID.	Cement (kg)	Fly ash (kg)	Slag (kg)	Water* (kg)	Nano-silica (kg)	BFP (kg)	Fine aggregate (kg)	HRWR (l)
F-2.5	350	350	--	210	--	43.3	1,130	2.5

N-F-2.5	350	350	--	180	84	43.3	1,045	5.6
N-F-4.5	350	350	--	180	84	78.3	1,000	5.0
G-2.5	350	--	350	210	--	43.3	1,245	6.0
N-G-2.5	350	--	350	180	84	43.3	1,160	7.6
N-G-4.5	350	--	350	180	84	78.3	1,100	7.3

*Adjusted amount of mixing water considering the water content of nano-silica (aqueous solution with 50% solid content of SiO_2).

The ingredients were mixed according to Azzam *et al*. (2019) [9]. After casting, the specimens were covered with a polyethylene sheet, and demolded after 24 hours. Subsequently, the specimens were stored at 22±2°C and at least 95% relative humidity (RH) in a curing room until the age of testing.

2.2. Testing

The mechanical properties of the composites were evaluated through the compressive strength at 1, 3, 7, 28, 56, and 90 days using triplicate cylinders of 100 mm diameter and 200 mm length in accordance with ASTM C39 [17]. Moreover, the flexural strength and toughness of the composites at 56 days was determined according to ASTM C1609/C1609M [18] using triplicate 100×100×350 mm prisms. The composites' resistance to infiltration of fluids was evaluated via the rapid chloride penetrability test (RCPT), according to ASTM C1202 [19], on triplicate discs (100 mm diameter and 50 mm length). Subsequently, the RCPT disc specimens were split into two halves, and 0.1 M silver nitrate solution was sprayed on the split faces giving a white precipitate of silver, where the average penetration depth of this precipitate was measured [20].

To evaluate the compatibility between the composites and substrate concrete, coefficient of thermal expansion (CTE), and pull-off tests were performed. CTE was determined according to AASHTO T336 [21] using triplicate cylinders with 100 mm diameter and 178 mm length for each mixture at 56 days. The pull-off test was carried out according to CSA A23.2-6B [22], where duplicate slabs (250×250×130 mm) of parent concrete were prepared to serve as a substrate layer. The parent concrete for these slabs was a typical concrete pavement mixture used in Manitoba [23] (400 kg/m3 GU cement with 15% fly ash replacement at *w/b* of 0.4). The parent concrete was kept in the curing room (22±2°C and at least 95% RH) for 7 days followed by storage in laboratory (22±2°C and at least 55±5% RH) for 180 days to eliminate residual shrinkage strain. Subsequently, the surfaces of the slabs were mechanically roughened, wire brushed, cleaned, and misted to acting as the substrate layer. The cementitious composite repair/overlay layer, 70 mm, was poured on the parent concrete, where it represents approximately one-third of the total assembly thickness. Two additional slabs were prepared for each of the N-F-4.5 and N-G-4.5 mixtures to investigate the influence of bonding agents (commercial acrylic grout "BG" and NS sol) on the bond strength of the assembly. The slabs were partially cored at 56 days from casting the repair/overlay layer to assess the bond between the composites and parent concrete.

The microstructure of composites was investigated using an environmental scanning electron microscope (ESEM) with elemental disperse X-ray (EDX) on fracture pieces from specimens.

3. Experimental Results and Discussion

3.1. Mechanical Properties and Hydration Development

The average compressive strengths as well as the flexural performance parameters of the composites are presented in Figs. 2 and 3. Blended binders incorporating high-volumes Type F fly ash (slowly reactive pozzolan) or slag (latent hydraulic binder) typically exhibit slow rate of strength and microstructural development at early-age, yet, their reactivity improve with time [11]. Thus, most standards and codes [e.g., 16] require the assessment of such concrete at 56 or 91 days. The compressive strength of all composites at early-age was high, due to the high binder content and low *w/b*. The nano-modified composites achieved compressive strength in the range of 30 to 48 MPa and 37 to 63 MPa at 1 and 3 days, respectively. These ranges, for example, meet the requirements (minimum strength of 15 to 25 MPa) of rapid repair and fast-tracked overlays applications in concrete pavements and bridge decks [1,2,4,23]. Moreover, the average increase in compressive strength at early ages (1, 3, 7 days) for nano-modified mixtures N-F-2.5 and N-G-2.5 was 25% and 17%, respectively relative to that of the reference mixtures F-2.5 and G-2.5. The ultrafine nature of NS (80,000 m2/kg) accelerated the hydration process of cement through providing additional nucleation sites [24]. In addition, colloidal NS solutions were found to create silica-agglomerates imparting a filler effect in the cementitious matrix [25]. Kong *et al*. [24] observed that water could be absorbed in the high nano-porosity of NS agglomerates, thus decreasing the *w/b* in the paste and in turn densifying the pore structure.

The nano-modified composites continued gaining later-age compressive strength, though at lower rates (Fig. 2). Correspondingly, addition of NS improved the flexural performance of the composites at 56 days (Fig. 3). The first-cracking flexural strength of N-F-2.5 and N-G-2.5 was increased by 8% and 13% relative to that of the reference mixtures without NS, and toughness was increased by 16% and 35%, respectively. The slower later-age strength evolution for the nano-modified composites was ascribed to the long-term pozzolanic reactivity of fly ash/slag and filling effect of NS particles. The ranges of compressive strength at later ages highlight the adequacy of the composites for repair/overlay applications, as they comply or exceed the strength requirements (30 to 65 MPa at 28 or 56 days) for repair/overlay in concrete pavements and bridges [e.g., 4,26,27].

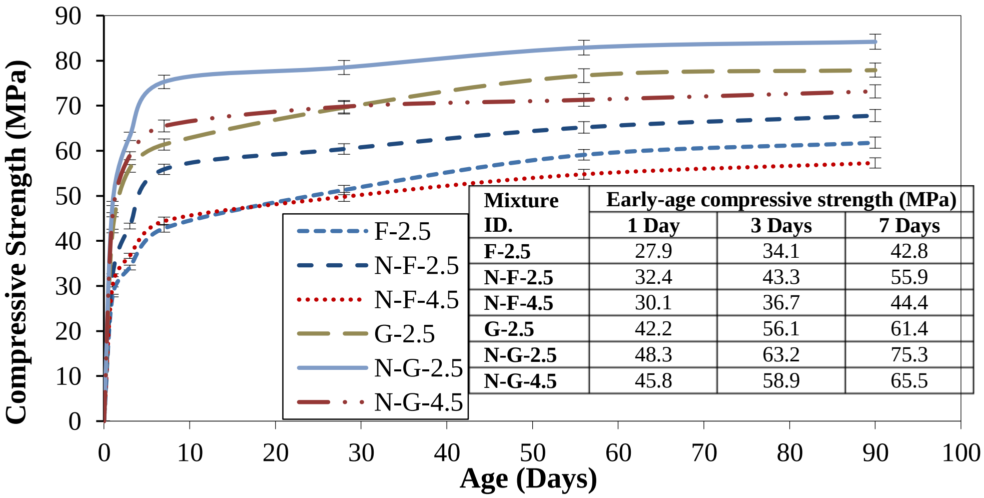

Mixture ID.	Early-age compressive strength (MPa) 1 Day	3 Days	7 Days
F-2.5	27.9	34.1	42.8
N-F-2.5	32.4	43.3	55.9
N-F-4.5	30.1	36.7	44.4
G-2.5	42.2	56.1	61.4
N-G-2.5	48.3	63.2	75.3
N-G-4.5	45.8	58.9	65.5

Fig. 2: Compressive strength versus time. (Note: error bars represent standard deviations).

The slag-based composites had higher mechanical properties relative to that of their fly ash-based counterparts (Figs. 2 and 3). This can be ascribed to the higher reactivity of slag relative to fly ash, which enhanced level of maturity of slag-based binders and in turn mechanical properties. Correspondingly, the improved reactivity of the slag-based composites resulted in higher quality of the ITZ (calcium to silicate ratio [*Ca/Si*] of 1.16) at BFP/matrix interface relative to fly-ash mixtures (*Ca/Si* of 1.37) (Fig. 4), consequently, better interfacial bond strength. The *Ca/Si* of C-S-H from the pozzolanic reaction tends to 1.1, whereas primary C-S-H generated from cement hydration reactions tends to 1.7 [11].

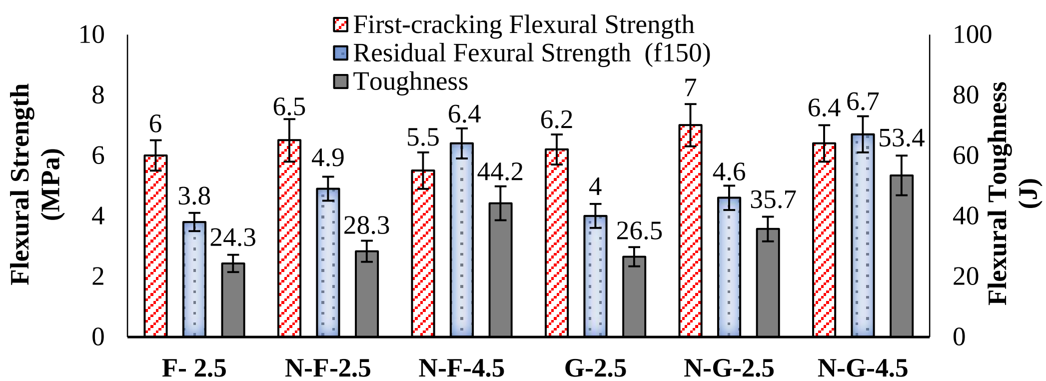

Fig. 3: Flexural parameters of the composites at 56 days. (Note: error bars represent standard deviations).

Increasing the dosage of BFP from 2.5% to 4.5% led to decreasing the compressive and first-cracking flexural strengths values (Figs. 2 and 3). For instance, the compressive strength of the nano-modified composites N-F-4.5 and N-G-4.5 at 28 days was reduced by 18% and 11%, respectively relative to that of their counterparts with the lower BFP dosage (2.5%), and the first-cracking flexural strength was reduced by 15% and 9%, respectively. This can be linked to the increase of air content and creation of additional interfacial transitional zones (ITZs) with the higher dosage of BFP, which represented weak links and stress concentrators in the matrix, thereby decreasing its capacity. However, these aspects did not reduce the early- and later-age strength of the composites below the typical requirements requirements for repair and overlay applications in concrete pavements and bridges, as outlined earlier. Moreover, the minimum flexural strength for the composites was 5.5 MPa, which is higher than the minimum requirement (4.5 MPa) for concrete overlays commonly stipulated by transportation agencies [e.g., 4].

The cementitious composites had high toughness and residual strengths, even at the lower BFP dosages (Fig. 3), complying with the guidelines' requirements for overlay systems comprising fiber reinforced cementitious materials, which stipulate an average residual strength (f_{150}) of 0.7 to 4.5 MPa [e.g., 4]. This is attributed to the designed microgrooves on the pellets' surface in the longitudinal direction which imparted an interlocking effect between the matrix and pellets, through increasing the contact surface and providing host locations for deposition of hydration products (Fig. 4). This resulted in high resistance to pull-out of BFP, which is the key toughening mechanism responsible for improving the ductility of composites. Increasing the BFP dosage in the composites significantly enhanced the toughness of composites and their residual strength (Fig. 3). The toughness of composites N-F-4.5 and N-G-4.5 was increased by 56% and 50%, respectively relative to that of their corresponding mixtures with 2.5% BFP. This is ascribed to abundance of pellets at cracking planes, which arrested cracks resulting in strain hardening beyond the first-cracking stage. The enhanced ductility of the composites may allow for thinner overlays or longer transverse joint spacing in jointed overlays.

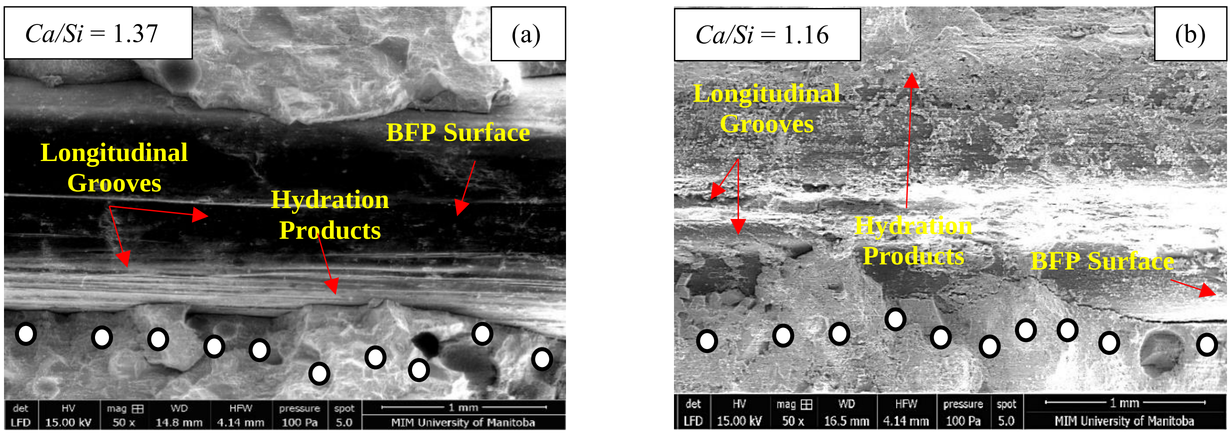

Fig. 4: Exemplar SEM micrographs for the nano-modified composites at 56 days showing ITZ with BFP in: (a) N-F-2.5, and (b) N-G-2.5. (Note: Ca/Si value is the average for the EDX analysis at marked locations).

3.2. Penetrability Features

The penetrability parameters of the composites are summarized in Table 2. All composites had passing charges less than 1000 coulombs, and thus 'very low' penetrability, in accordance with ASTM C1202 classification. This can be ascribed to the mixture design of the composites (high binder content and low *w/b*), which produced dense cementitious matrix. Various guidelines and specifications for repair and overlay systems in concrete pavements and bridges require low penetrability to reduce moisture infiltration/saturation into the cementitious matrix, thus improving its durability against chemical and/or physical mechanisms (e.g., de-icing salt and/or frost action). For example, the recommended maximum passing charges for such applications at 56/90 days is less than 1500/1000 coulombs [1,2,26].

The physical penetration depth, which ranged between 4.6 and 14.6 mm, indicated differences in microstructural features among composites based on the type of binder and BFP dosage, complying with the trends of mechanical properties. For instance, addition of NS to mixtures N-F-2.5 and N-G-2.5 decreased the physical penetration depth by 33% and 49%, respectively relative to that of the reference composites. These trends highlight the functionality of NS with high-volume SCM binders at improving the maturity level and densifying the cementitious matrix, as discussed earlier.

Increasing the BFP dosage led to higher penetrability in the composites (Table 2). For instance, the physical penetration depths in N-F-4.5 and N-G-4.5 specimens were 11% and 26%, respectively higher than that of their corresponding specimens with the lower BFP dosage (2.5%). The foaming action observed during mixing of BFP with other ingredients led to increasing the air content of composites with dosage, especially with the absence of coarse aggregate and higher viscosity of the composites in the fresh state relative to conventional concrete [11]. This led to preventing some air bubbles from rising to the surface during vibration. Moreover, increasing the BFP dosage led to the formation of additional ITZs, which contributed to the relatively coarser microstructure of the matrix and increased penetrability. However, all composites herein had 'very low' penetrability, regardless of the BFP dosage, which indicate high resistance to exposures involving intrusion of fluids.

Table 2: Penetrability results at 56 days

Mixture ID.	RCPT parameters		
	Passing charges (coulombs)	Chloride ion penetrability class (ASTM C1202)	Physical chloride penetration depth (mm)
F- 2.5	980	Very Low	14.6 (2.8)
N-F-2.5	630	Very Low	9.8 (2.6)
N-F-4.5	684	Very Low	10.9 (2.1)
G-2.5	688	Very Low	9.1 (2.3)
N-G-2.5	348	Very Low	4.6 (0.5)
N-G-4.5	379	Very Low	5.8 (0.8)

Notes: Numbers in brackets indicate standard deviations.

3.3. Compatibility with Substrate Concrete

3.3.1. Coefficient of Thermal Expansion

The coefficients of thermal expansion (CTE) of the composites were calculated, where the fly ash-based mixtures had an average CTE of 10.6×10^{-6}/°C, while it was 10.1×10^{-6}/°C for the slag-based mixtures. The CTE of the cementitious composites was found to be comparable to that of the parent concrete, where the parent concrete had a CTE value of 10.9×10^{-6}/°C. Hence, this indicates thermal compatibility between both components of the repair/overlay system. These narrow range of results for CTE with parent concrete comply with recommendations of various guidelines for repair/overlay systems [1,2,4] to mitigate the detrimental effects (cracking, poor bonding, delamination) of thermal mismatch between the topping material and parent concrete.

The inclusion of NS and type of binder (fly ash/slag) had insignificant effects on the CTE of the composites, where F-2.5 and N-F-2.5 had CTE of 11.1×10^{-6}/°C and 10.9×10^{-6}/°C, respectively, while G-2.5 and N-G-2.5 had CTE of 10.6×10^{-6}/°C and 10.1×10^{-6}/°C. This conforms to previous studies [11] that reported CTE values of mortar with siliceous sand ranging between 10 to 12×10^{-6}/°C according to the volume ratio of the sand, with marginal effects of *w/b* and binder type. The presence of stiff macro-BFP (elastic modulus of 65 GPa), randomly oriented in the matrix, restrained the thermal deformations of high volume of paste in the composites, thus compensating for the absence of coarse aggregate and keeping close CTE ranges to that of normal substrate concrete. Increasing the BFP dosage in the matrix further restrained its volumetric change due to thermal gradients, albeit to a marginal extent. Thus, the CTE of mixtures N-F-4.5 (9.8×10^{-6}/°C) and N-G-4.5 (9.6×10^{-6}/°C) was reduced by 10% and 5%, respectively compared to that of their counterpart mixtures with 2.5% BFP dosage. This insignificant reduction of CTE could also be attributed to the inclusion of more BFP with low CTE (1.4×10-6/°C) in the matrix.

3.3.2. Bond Strength

The bond strength between the proposed composites and parent concrete was evaluated and the results were presented in Fig. 5. All composites, without bonding agents, had bond strength in the narrow range 1.59 to 1.89 MPa, and the failure of the assembly took place in the substrate layer (10 to 70 mm below the interface). This indicated efficient compatibility between the two layers and integrity of the proposed repair/overlay systems. The bond strength had a narrow range as it represented the tensile strength of the substrate layer (parent concrete) in the test assembly (weakest link). The trend can be ascribed to the adequate curing period of the composite layer, resulting in significant hydration and microstructural development of the matrix, which was reflected on the interfacial bonding between the repair/overlay and substrate layers. Moreover, it indicated that there was no preferential plastic sedimentation of BFP towards the interface, which would have otherwise caused de-bonding at the interface.

The bond strength of the assembly comprising the bonding grout at the interface of N-F-4.5(BG) and N-G-4.5(BG) showed comparable values to that of the corresponding assemblies without bonding agent (Fig. 5), and the failure occurred in the substrate layer (i.e., high compatibility). On the contrary, the use of NS colloid as a coating at the interface compromised the integrity of the repair/overlay system. The bond strength of N-F-4.5(NS) and N-G-4.5(NS) were 43% and 26% less, respectively, relative to that of corresponding assembly without NS interfacial coating, where the failure occurred at the interface between the two layers due to low compatibility. It is suggested that when NS colloid was applied at the interface, the remaining/unreacted NS formed a condensed layer at the interface acting as a separator, which impaired the adhesion between the two layers of the assembly.

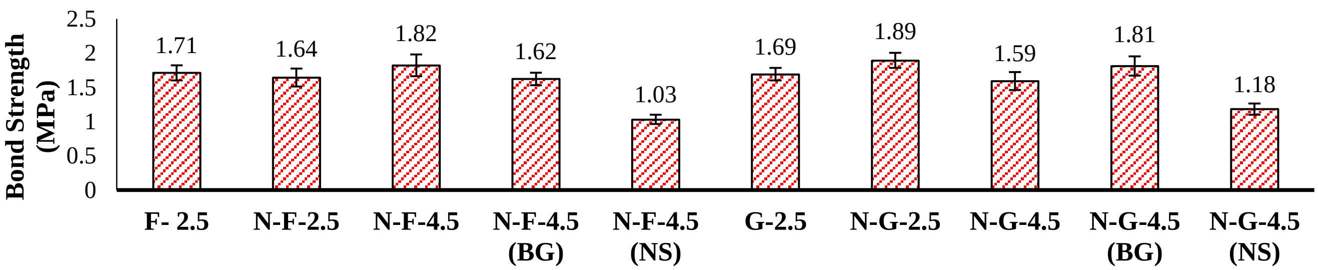

Fig. 5: Bond strength of the repair/overlay assembly. (Note: error bars represent standard deviations; BG and NS denote bonding grout and nano-silica colloid applied at the interface).

4. Conclusion

Considering the mixtures design, type of fibers (BFP), and scope of tests in this study, the following conclusions can be drawn:

- The compressive strength trends captured the catalytic and synergistic effects of NS with fly ash/slag on improving early-age and later-age compressive strength of the composites. Hence, at 1 day, the nano-modified cementitious composites exceeded 30 MPa, and at 56 days, they exceeded 50 MPa with a minimum flexural strength of 5.5 MPa, complying with typical strength requirements for repair/overlay applications in concrete pavements and bridge decks.
- Despite the adverse effect of increasing the BFP dosage on reducing the mechanical capacity of nano-modified composites, it improved their ductility, due to the abundance of BFP at the failure plane and deposition of hydration products in the BFP surface microgrooves that enhanced the efficiency of pull-out process.
- The slag-based composites exhibited higher mechanical properties and resistance to infiltration of fluids, relative to the fly ash-based composites, due their improved reactivity/maturity and densified microstructure. However, all the nano-modified cementitious composites, met the mechanical (strength ranges) and durability (very low penetrability) requirements for repair/overlay applications.
- The cementitious composites showed high thermal compatibility with substrate concrete, owing to the restraining role of BFP. Moreover, the composites had efficient integrity/continuity (bond strength) with the substrate concrete, without requiring bonding agents, where the substrate mode of failure was dominant.

Acknowledgements

The authors appreciate the financial support from the Natural Sciences and Engineering Research Council of Canada (NSERC RGPIN/4024-2020) and University of Manitoba Research Grants Program (URGP 2019/2020).

References

[1] D. P. Frentress and D. S. Harrington, “Guide for partial-depth repair of concrete pavements,” Iowa State University Institute for Transportation, 2012, 33 p.

[2] D. Harrington and G. Fick, “Guide to Concrete Overlays: Sustainable Solutions for Resurfacing and Rehabilitating Existing Pavements, 3rd Edition,” Iowa State University Institute for Transportation, 2014, 145 p.

[3] American Concrete Institute, ACI PRC-546R-14, “Concrete Repair Guide,” Farmington Hills, MI, USA, 2014, 70 p.

[4] American Concrete Institute, ACI PRC-325.13-06, “Concrete Overlays for Pavement Rehabilitation (Reapproved 2020),” Farmington Hills, MI, USA, 2006, 39 p.

[5] H. Soliman and A. Shalaby, "Characterizing the Performance of Cementitious Partial-Depth Repair Materials in Cold Climates," *Constr. Build. Mater.*, vol. 70, pp. 148-157, 2014.
[6] C. Jiang, K. Fan, F. Wu, and D. Chen, "Experimental study on the mechanical properties and microstructure of chopped basalt fibre reinforced concrete," *Mater. and Des.*, vol. 58, p. 187-193, 2014.
[7] J. J. Lee, J. Song, and H. Kim, "Chemical stability of basalt fiber in alkaline solution*," Fib. and Poly.*, vol. 15, no. 11, pp. 2329-2334, 2014.
[8] J. Branston, S. Das, S. Y. Kenno, and C. Taylor, "Mechanical behaviour of basalt fibre reinforced concrete," *Constr. Build. Mater.*, vol. 124, pp.878-886, 2016.
[9] A. Azzam, M. T. Bassuoni, and A. Shalaby, "Properties of High-Volume Fly Ash and Slag Cementitious Composites Incorporating Nanosilica and Basalt Fiber Pellets," *Adv. in Civ. Eng. Mater*., vol. 8, no. 3, pp. 255-274, 2019.
[10] V. M. Malhotra, M. H. Zhang, P. H. Read, and J. Ryell, "Long- Term Mechanical Properties and Durability Characteristics of High- Strength/High-Performance Concrete Incorporating Supplementary Cementing Materials Under Outdoor Exposure Conditions," *ACI Mater. J.*, vol. 97, no. 5, pp. 518-525, 2000.
[11] P. K. Mehta, and P. J. M. Monteiro, *Concrete: microstructure, properties, and materials*. McGraw Hill Education, 675 p, 2014.
[12] M. H. Zhang, J. Islam, and S. Peethamparan, "Use of nano-silica to increase early strength and reduce setting time of concretes with high volumes of slag," *Cem. Conc. Comp*., vol. 34, no. 5, pp. 650-662, 2012.
[13] ASTM C672/C672M, "Standard Test Method for Scaling Resistance of Concrete Surfaces Exposed to De-icing Chemicals," ASTM International, West Conshohocken, PA, 2012.
[14] A. Azzam, M. T. Bassuoni, and A. Shalaby, "Nanomodified Cementitious Composites Incorporating Basalt Fiber Pellets under Tensile and Impact Loads," *J. of Mater. in Civ. Eng*., vol. 33, no. 10, p. 04021260, 2021.
[15] CAN/CSA-A3001, "Cementitious Materials for Use in Concrete," Canadian Standards Association, Mississauga, Ontario, Canada, 691 p, 2018.
[16] CSA-A23.1/A23.2, "Concrete materials and methods of concrete construction/test methods and standard practices for concrete," Canadian Standards Association, Mississauga, Ontario, Canada, 2019.
[17] ASTM C39/C39M, "Standard Test Method for Compressive Strength of Cylindrical Concrete Specimens," ASTM International, West Conshohocken, PA, 2020.
[18] ASTM C1609/C1609M, "Standard Test Method for Flexural Performance of Fiber-Reinforced Concrete (Using Beam with Third-Point Loading)," ASTM International, West Conshohocken, PA, 2019.
[19] ASTM C1202, "Standard Test Method for Electrical Indication of Concrete's Ability to Resist Chloride Ion Penetration," ASTM International, West Conshohocken, PA, 2019.
[20] M. T. Bassuoni, M. L. Nehdi, and T. R. Greenough, "Enhancing the reliability of evaluating chloride ingress in concrete using the ASTM C 1202 rapid chloride penetrability test," *J. of ASTM Inter*., vol. 3, no. 3, pp. 1-13, 2005.
[21] AASHTO T336-15, "Standard Test Method for the Coefficient of Thermal Expansion of Hydraulic Cement Concrete," Washington, D.C., 2015.
[22] CSA A23.2-6B, "Determination of Bond Strength of Bonded Toppings and Overlays and of Direct Tensile Strength of Concrete, Mortar, and Grout," CSA A23.1/A23.2, Canadian Standards Association, Mississauga, ON, Canada, 2019.
[23] CW3310-R17, "Portland Cement Concrete Pavement Works," City of Winnipeg Specification, Winnipeg, Manitoba, Canada, 2015.
[24] D. Kong, X. Du, S. Wei, H. Zhang, Y. Yang, and S. P. Shah, "Influence of Nano-Silica Agglomeration on Microstructure and Properties of the Hardened Cement-Based Materials," *Constr. Build. Mater.*, vol. 37, pp. 707-715, 2012.
[25] T. Oertel, F. Hutter, R. Tänzer, U. Helbig, and G. Sextl, "Primary particle size and agglomerate size effects of amorphous silica in ultra-high performance concrete," *Cem. Conc. Comp*., vol. 37, pp. 61-67, 2013.
[26] City of Winnipeg Standard Construction Specifications, Winnipeg, Manitoba, Canada, 2021. [Online]. Available: https://www.winnipeg.ca/matmgt/spec/default.stm
[27] T. P. Wilson, K. L. Smith, and A. R. Romine, "LTPP pavement maintenance materials: PCC partial-depth spall repair experiment," Final Report (No. FHWA-RD-99-1 53), Turner-Fairbank Highway Research Center, 109 p, 1999.